ACI MATERIALS JOURNAL TECHNICAL PAPER

Title no. 106-M47

Influence of Material Ductility on Performance of Concrete Repair

by Mo Li and Victor C. Li

The lack of durability in concrete repairs induces premature repair deterioration. Drying shrinkage of "new" repair material restrained by "old" concrete substrate results in repair layer cracking, and interface delamination between the repair and the concrete substrate. This paper investigates a material solution to these common repair failures. A high-early-strength engineered cementitious composite (HES-ECC) developed for concrete repair is employed for this study. The HES-ECC possesses high early-age strength (over 47 MPa [6885 psi] in 7 days) and high tensile strain capacity several hundred times that of normal concrete or fiber-reinforced concrete (FRC). Experimental and numerical studies on a layered repair system were conducted to verify that the high ductility of HES-ECC can relieve shrinkage-induced stresses in the repair layer and at the repair/old concrete interface, thereby simultaneously suppressing large repair surface cracks and interface delamination. Detailed results of these studies are reported in this paper.

Keywords: cracking; ductility; durability; interface delamination; repair; shrinkage; simulation.

INTRODUCTION

A large number of existing concrete structures worldwide, including previously repaired ones, suffer from deterioration or distress under combined mechanical and environmental loading conditions.[1] These structures are in urgent need of repair. While more and more "durable" repair materials have been developed recently, concrete repair outcomes are highly variable. It has been estimated that almost half of all concrete repairs fail in the field.[2] Concrete repairs are often perceived to lack both early-age performance and long-term durability.[3]

Concrete repair failure results from a combination of physical, chemical, and mechanical processes.[4,5] Generally it is the restrained volume change due to drying shrinkage or the difference in thermal expansion coefficient that induces repair surface cracking and/or interface delamination between the repair and the old concrete. Surface cracking and interface delamination are causes of many repair durability problems.[6] They facilitate the ingress of chlorides, oxygen, moisture, alkali, or sulfates into the repaired system and accelerate further deterioration.[7] For example, chloride penetration is much faster through cracks in concrete cover than through sound concrete.[8] In overlay repair applications, delamination of concrete bridge overlays from the substrate deck is one of two primary causes of ultimate overlay failure.[9] The total cost, including repeated repairs over the structure's service life, can be several times greater than the initial cost of structural design and construction.[10]

This research investigates the performance of an ultra-ductile concrete—a high-early-strength engineered cementitious composite (HES-ECC)—as a repair material to improve durability of concrete structures. Engineered cementitious composite (ECC) is a fiber-reinforced cement based composite micromechanically tailored[11-15] to exhibit metal-like tensile response with ultra-high tensile strain capacity of 3 to 5%, approximately 300 to 500 times the tensile strain capacity of normal concrete and fiber-reinforced concrete (FRC). HES-ECC is a specialized version of ECC. It incorporates the function of developing compressive strength rapidly at material early age while maintaining high tensile ductility at both early and late ages. The high early strength property enables early returning of the repaired structure to service, while the tensile ductility is essential to achieving early-age performance and long-term durability throughout the repaired structure's service life. The durability of ECC/concrete repairs under mechanical loads has been studied previously.[16-18] This paper studies the durability of HES-ECC/concrete repairs under environmental load. It is suggested that minimizing repair layer surface cracking and repair/old concrete interface delamination due to restrained drying shrinkage can suppress the concrete repair deterioration process. The detailed material design of HES-ECC can be found in Wang and Li[19] and Li and Li.[20]

In this paper, findings from experimental and numerical studies carried out on simulated layered repair systems under controlled humidity are reported. Measurements of repair surface cracking and repair/old concrete interface delamination magnitude and extent confirm the effectiveness of simultaneously suppressing these two deterioration mechanisms when HES-ECC is used as the repair material. The underlying mechanisms for these performance benefits, not achievable by concrete and FRC, are also clarified.

RESEARCH SIGNIFICANCE

A material-based methodology using ductile HES-ECC is proposed and is experimentally and numerically validated in this study to improve durability of repaired concrete structures. This research departs from the traditional emphasis on high compressive strength of repair materials, and moves toward a balance of strength, ductility, and repair material's compatibility with existing concrete. When the tensile ductility requirement is satisfied, repair material's free shrinkage limit and crack-control reinforcements become less important. This concept of translating repair material ductility to repair system durability can be widely applied to many concrete repair applications for minimizing maintenance requirements and reducing repair costs.

ACI Materials Journal, V. 106, No. 5, September-October 2009.
MS No. M-2008-188.R1 received June 12, 2008, and reviewed under Institute publication policies. Pertinent discussion including authors' closure, if any, will be published in the July-August 2010 *ACI Materials Journal* if the discussion is received by April 1, 2010.

ACI member **Mo Li** *is a PhD Candidate and Research Assistant in the Department of Civil and Environmental Engineering at the University of Michigan, Ann Arbor, MI. She received her BSE from Tongji University, China, and her MSE from the University of Michigan. Her research interests include concrete repair durability, composite material development for sustainable infrastructure, and corrosion in reinforced or prestressed concrete structures.*

ACI member **Victor C. Li** *is a Professor in the Department of Civil and Environmental Engineering at the University of Michigan. He is a member of ACI Committee 544, Fiber Reinforced Concrete. His research interests include the analysis, modeling, and design of ultra-ductile and green cementitious composites, their application to innovative and sustainable infrastructure systems, and integration of materials and structural design.*

Table 1—Mixture proportion of HES-ECC

HES-ECC mixture design parameter	Value, kg/m^3 (lb/ft^3)
Portland cement, Type III	918.0 (57.31)
U.S. silica sand, F110	918.0 (57.31)
Water	300.7 (18.77)
Polyvinyl alcohol fiber	26.1 (1.63)
Polystyrene beads	58.8 (3.67)
High-range water-reducing admixture	6.9 (0.43)
Accelerating admixture	36.7 (2.29)
Hydrating control admixture	Optional

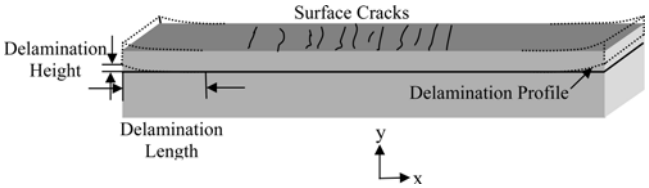

Fig. 1—Schematics of typical failure modes in layered repair system.

BACKGROUND

In concrete repair applications, the early-age shrinkage deformation of the "new" repair material after placement is restrained by the "old" concrete substrate that has already undergone shrinkage. Consequently, tensile stress is developed in the repair layer, and a combination of tensile and shear stresses is built up along the interface between the repair and the concrete substrate. Tensile stress at repair/substrate interface is the y-direction stress that opens the interface (which delaminates the interface in the y-direction [Fig. 1]). Shear stress at repair/substrate interface is the x-direction stress that causes the repair layer to slide along the surface of the substrate (which delaminates the interface in the x-direction [Fig. 1]). These stresses can cause repair surface cracking and/or interface delamination, as schematically illustrated in Fig. 1. The crack width and delamination magnitude determine the transport properties through this repair system and are therefore closely related to repair durability. A detailed discussion on stress distribution and failure mechanism in a concrete repair system undergoing drying shrinkage can be found in Wittmann and Martinola.[21]

Li and Stang[22] proposed the concept of cracking potential p for concrete materials under restrained shrinkage, where p is defined as

$$p = (\varepsilon_{sh} - (\varepsilon_e + \varepsilon_{cp})) \quad (1)$$

and ε_{sh} is the material's shrinkage strain, ε_e is its elastic tensile strain capacity, and ε_{cp} is its tensile creep strain. ε_{sh}, ε_e, and ε_{cp} are expressed as positive values and are time dependent. Therefore, p is also a time-dependent variable. ε_{sh} can be extended to the more general case of total imposed strain due to drying shrinkage, autogeneous shrinkage, and thermal effect. At any given time, a high positive value of p signifies a strong potential for cracking due to restrained shrinkage. After a crack forms, its width will depend on p, structural dimensions, and steel reinforcement ratio.

For a repair layer, restraint from the substrate may result in a high p-value leading to repair layer surface cracking. Through the formation and opening of these cracks, stresses built up in the repair layer, and especially at the interface, can be relaxed. By this means, interface delamination tendency is greatly reduced.

Fibers have been used in concrete repairs to control cracking. For tension-softening FRC materials, shrinkage-induced stresses can result in surface cracking similar to concrete. These cracks, however, are restrained by the bridging fibers, so that the shrinkage-induced stresses are not fully relaxed. As a result, interface delamination can be more prominent in FRC repairs than in concrete or mortar repairs. This phenomenon was first observed by Kabele[23] through a numerical study of repair systems involving concrete and FRC.

To suppress both repair surface cracking and repair/old concrete interface delamination, the repair material needs to exhibit "inelastic straining" to accommodate its shrinkage deformation, thus relieving the stresses built up under restrained drying shrinkage conditions. By this means, surface crack width and interface delamination can be both minimized. Inelastic straining in the form of microcrack damage has been demonstrated in HES-ECC that was developed for this study.[20] This inelastic deformation behavior of HES-ECC is exploited in the present study of repair durability. It should be noted that in ECC, even though the cracks are also not traction-free as in FRC, and are in fact much tighter in width, the much larger number of these microcracks gives rise to the inelastic straining that leads to relaxing the built-up stress due to restrained shrinkage. The mixture ingredients and proportion of HES-ECC are shown in Table 1.

HES-ECC has been optimized to have large values of inelastic tensile strain capacity ε_i at minimum fiber content. For HES-ECC, the cracking potential[24] is modified as

$$p = (\varepsilon_{sh} - (\varepsilon_e + \varepsilon_i + \varepsilon_{cp})) \quad (2)$$

Figure 2 shows the typical uniaxial tensile stress-strain curve of HES-ECC at different ages (4 hours, 24 hours, 3 days, 7 days, 28 days, and 60 days). Specimens were 228.6 mm (9 in.) in length, 76.2 mm (3 in.) in width, and 12.7 mm (0.5 in.) in thickness, demolded after 4 hours (for the specimens tested at 4 hours) or 6 hours (for the specimens tested at later ages), and cured in air. The end points of each curve represent the beginning of fracture localization after the ultimate tensile strength and strain capacity have been reached. Fracture localization refers to localization of deformation by widening of a single crack while the tensile load-bearing capacity drops. The high ductility and tensile strain capacity (>3%) of HES-ECC is achieved by forming many closely spaced microcracks after first crack and before fracture localization.

It was observed that specimens at all ages were nearly "saturated" with closely-spaced microcracks with crack widths less than 70 mm (2.76×10^{-3} in.). It should be noted that

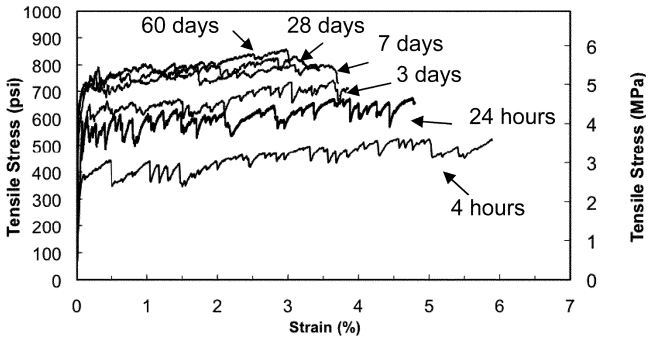

Fig. 2—HES-ECC tensile stress-strain curves at different ages.

the crack width at the very early age of 4 hours is as low as 10 μm (0.39×10^{-3} in.). Due to the designed fiber bridging,[4] these microcracks carry increasing traction without increasing crack width after achieving a "steady state"—a condition to achieve ECC multiple-cracking and strain-hardening behavior (Fig. 2). A previous study[25] of ECC tensile strain capacity up to 180 days indicates that the material reaches a long-term strain capacity of 3% beyond 90 days. The age-dependent properties of HES-ECC are further discussed in the following.

The formation of many fine microcracks in HES-ECC can be regarded as inelastic straining on the macroscopic repaired-system-size scale. The large value of ε_i (>3%) for HES-ECC gives a highly negative cracking potential p in Eq. (2), suggesting that localized fracture due to restrained shrinkage will be inhibited. Instead, the repair material will undergo inelastic straining by developing multiple microcracks with controlled crack width. Therefore, HES-ECC is suggested to be a promising material for durable repair jobs by minimizing repair surface cracking and interface delamination.

EXPERIMENTAL INVESTIGATION

Materials

Three different repair materials—HES-concrete, HES-steel fiber-reinforced concrete (HES-SFRC) with tension softening behavior, and HES-ECC with strain-hardening behavior—were investigated in this study. The HES-concrete and HES-SFRC were employed as controls. All three materials used Type III high-early-strength portland cement. Mixture proportions are summarized in Table 2.

Age-dependent tests in uniaxial tension were conducted on HES-ECC, HES-concrete, and HES-SFRC plate specimens. The direct uniaxial tensile test is considered the most convincing method to evaluate material strain-hardening behavior.[26] The plate specimens measuring 228.6 mm (9 in.) in length, 76.2 mm (3 in.) in width, and 12.7 mm (0.5 in.) in thickness were tested in an MTS machine with 25 kN (5.62 kip) capacity under displacement control at a rate of 0.005 mm/s (1.97×10^{-4} in./s). Two external linear variable displacement transducers (LVDTs) were attached to the specimen surface with a gauge length of 101.6 mm (4 in.) to measure the displacement. Specimens were demolded after 6 hours and then cured in air to simulate early exposure to traffic field conditions. Six specimens of each mixture were tested at different ages. Their material mechanical properties are reported in Table 3.

The HES-concrete repair layer and the concrete substrate had the same material composition, except that the concrete substrate used ordinary concrete containing Type I portland cement whereas the HES-concrete repair used Type III portland cement. The HES-concrete mixture consisted of crushed limestone coarse aggregate (CA) with 14 mm (0.55 in.) nominal grain size, Type III portland cement (C), sand (S), and water (W). Superplasticizer (SP) (also known as high-range water-reducing admixture) was used to ensure sound workability. An accelerating admixture (AC) was used to accelerate the material's strength development and setting processes. The HES-concrete specimens were tested to have average compressive strength f_c' of 49.9 MPa (7234 psi) at the age of 7 days, and 53.0 MPa (7860 psi) at the age of 28 days. Under uniaxial tensile loading, the HES-concrete is a brittle material with sudden fracture failure.

The HES-SFRC mixture had the same composition as the concrete mixture, except that it contained 1% by volume of steel fibers. The steel fiber, with a length of 30 mm (1.18 in.) and a diameter of 0.5 mm (0.02 in.), had a smooth surface and hooked ends. The averaged 7- and 28-day compressive strengths of the HES-SFRC were 51.5 and 56.9 MPa (7462 and 8254 psi), respectively. Under tensile loading, the HES-SFRC is a quasi-brittle material with tension-softening behavior. Both the HES-concrete and the HES-SFRC had ultimate tensile strain capacity ε_u of around 0.01%.

The HES-ECC mixture is composed of Type III portland cement, water, silica sand with 110 μm (3.94×10^{-3} in.) nominal grain size, polystyrene beads with a size of 4 mm (0.157 in.) as coarse aggregates, superplasticizer, accelerating admixtures, and 2% by volume of polyvinyl alcohol (PVA) fibers. These PVA fibers had a length of 12 mm (0.472 in.) and diameter of 40 μm (1.54×10^{-3} in.). The HES-ECC fresh material is self-consolidating. Due to their weak bond with cementitious matrix, the polystyrene beads serve as deliberately introduced initial flaws to assist in triggering the multiple microcracks[19] during tensioning of the composite. The HES-ECC mixture had an averaged compressive strength of 47.5 MPa

Table 2—Repair materials composition

Material	C*	W	S	CA	SP	AC	V_f
HES-concrete	1.0	0.4	1.3	1.3	0.005	0.04	—
HES-SFRC	1.0	0.4	1.3	1.3	0.005	0.04	0.01‡
HES-ECC	1.0	0.33	1.0	0.064†	0.0075	0.04	0.02§

*Type III portland cement.
†Polystyrene beads as "coarse aggregates" for HES-ECC.
‡Steel hooked-end fiber.
§PVA fiber.
Note: C = cement; W = water; S = sand; CA = course aggregates; SP = high-range water-reducing admixture (superplasticizer); AC = accelerating admixture; V_f = fiber volume fraction. All numbers are given in weight ratios to cement, with the exception of V_f.

Table 3—Repair material mechanical properties

Material	Age, days	f_c'*, MPa (psi)	E*, GPa (ksi)	ε_u, %	Tensile behavior
HES-concrete	7	49.9 ± 1.6 (7234 ± 228)	26.2 ± 1.4 (3803 ± 196)	0.01	Brittle
	28	53.0 ± 2.4 (7860 ± 345)	27.8 ± 1.5 (4025 ± 221)		
HES-SFRC	7	51.5 ± 2.4 (7462 ± 348)	25.7 ± 2.0 (3725 ± 287)	0.01	Quasi-brittle
	28	57.0 ± 2.0 (8254 ± 290)	29.2 ± 1.3 (4231 ± 189)		
HES-ECC	7	47.5 ± 1.9 (6885 ± 275)	20.6 ± 0.7 (2986 ± 101)	3 to 5	Ductile
	28	55.6 ± 2.2 (8063 ± 315)	23.2 ± 1.0 (3365 ± 140)		

*Mean ± standard deviation.

Table 4—HES-ECC tensile properties at different ages

Age	E^*, GPa (ksi)	Tensile strength*, MPa (psi)	Strain capacity*, %
4 hours	13.10 ± 0.77 (1900 ± 111)	3.46 ± 0.08 (501 ± 12)	5.97 ± 0.22
6 hours	14.98 ± 0.79 (2173 ± 114)	4.21 ± 0.13 (610 ± 19)	4.97 ± 0.38
12 hours	16.05 ± 1.02 (2328 ± 147)	4.57 ± 0.17 (662 ± 25)	4.41 ± 0.33
24 hours	18.30 ± 0.59 (2654 ± 85)	4.69 ± 0.08 (680 ± 12)	3.99 ± 0.27
7 days	20.59 ± 0.70 (2986 ± 101)	5.56 ± 0.11 (807 ± 16)	3.52 ± 0.29
28 days	23.20 ± 0.96 (3365 ± 140)	5.68 ± 0.14 (823 ± 20)	3.47 ± 0.62

*Mean ± standard deviation (measured from nine specimens for each of the properties).

(6885 psi) at the age of 7 days, and 55.6 MPa (8063 psi) at the age of 28 days. Its averaged Young's modulus was 20.6 GPa (2986 ksi) at 7 days, and 23.2 GPa (3365 ksi) at 28 days, which was lower than that of the HES-concrete (26.2 GPa [3803 ksi] at 7 days and 27.8 GPa [4025 ksi] at 28 days), and the HES-SFRC (25.7 GPa [3725 ksi] at 7 days and 29.2 GPa [4231 ksi] at 28 days) due to the absence of coarse aggregates in its composition. A lower modulus repair material is, in fact, desirable in limiting the tensile stress induced by restrained drying shrinkage. Details on the design and development of this HES-ECC are reported in a separate paper under preparation.

Because drying shrinkage is a time-dependent process, it is necessary to evaluate the development of the HES-ECC's tensile strain capacity at different ages. Direct tensile tests were conducted from material age of 4 hours up to 60 days. The test results (Fig. 2) show that the HES-ECC's tensile strain capacity changes with age, due to the subtle competition between the time-dependent changes of the matrix toughness and the fiber/matrix interface bond properties. However, the tensile strain hardening behavior of the HES-ECC with a strain capacity larger than 3% can be maintained at all ages. The age-dependent tensile properties of the HES-ECC are summarized in Table 4.

Repair specimen configuration and surface preparation

In this study, layered repair systems were experimentally investigated with the three different repair materials described previously: HES-concrete, HES-SFRC, and HES-ECC. Concrete substrates were initially cast with dimensions of 1600 x 100 x 100 mm (63 x 4 x 4 in.), as shown in Fig. 3. They were moist-cured until the age of 28 days and then left to dry in an ambient condition of 15 to 21 °C (60 to 70 °F) and 35 to 55% relative humidity (RH) for an additional 150 days before the repair layers were placed. A free shrinkage test was conducted on three control specimens made from the same mixture as the substrate concrete under the same ambient condition. It showed that the shrinkage of the substrate concrete tapers off after 30 days, which indicated that the additional 150 days allowed for any potential shrinkage in the substrates to occur before bonding the repairs. This procedure was followed to simulate the conditions of actual repair of old concrete structures.

The contact surfaces of the concrete substrates were roughened in fresh state using a chisel to remove slurry cement from external surfaces of coarse aggregates. The estimated roughness amplitude was 3.8 to 5.1 mm (0.15 to 0.20 in.). Before placing the repair layer, the substrate surface was recleaned with a brush and high-pressure air to ensure a clean bonding surface, and then it was dampened with water fog. The moisture level of the contact surface was critical to achieve bond; excessive moisture in a contact surface may clog the pores and prevent absorption of the repair material. On the other hand, overly dry substrate contact surface may absorb water from the repair material, resulting in undesirable magnitude of shrinkage.[5] After dampening the surface, a 50 mm (2 in.) thick repair layer made of each of the three repair materials was cast on top of the concrete substrate. The repair layers were moist cured for 6 hours and then demolded. This curing condition and demolding time simulated early exposure to traffic field conditions. After demolding, the layered specimens were moved into a room with ambient conditions of 15 to 21 °C (60 to 70 °F) and 35 to 55% RH.

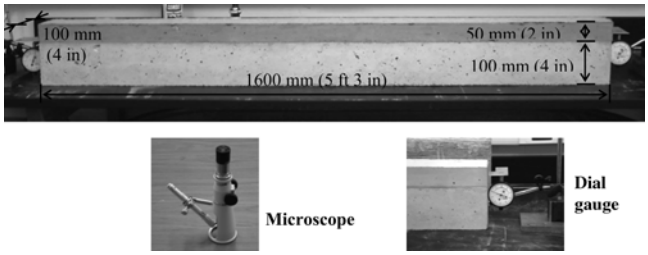

Fig. 3—Layered repair system test setup under restrained shrinkage.

For each specimen, two dial gauges (Fig. 3) were used to record interface vertical separation distance at end locations of the specimens as a function of drying time after delamination begins. In addition, a portable microscope was used to measure the delamination at 30 different locations along the interface, from which the delamination crack profile was derived. The microscope was also employed to observe crack pattern, crack number, and crack width of the top surface of the repair layer, as a function of age. Both the delamination and the surface cracking were measured daily until the age of 60 days.

Free shrinkage tests were also carried out to characterize free shrinkage properties of the HES-concrete, HES-SFRC, and HES-ECC mixtures. The free shrinkage test specimens were from the same batch as the repair layer mixture for each of the three repair materials. The tests were conducted according to ASTM C157/C157M-99[27] and ASTM C596-01[28] standards, except that the storing and testing environments of the specimens were modified to be the same as the layered specimens, with ambient conditions of 15 to 21 °C (60 to 70 °F) and 35 to 55% RH. The same storing and testing environments were used for relating the free shrinkage test results to the observed behavior of the layered specimens.

EXPERIMENTAL RESULTS AND DISCUSSION

Shrinkage of repair materials

Three specimens were tested for each of HES-ECC, HES-concrete, and HES-SFRC. The average free shrinkage strain ε_{sh} values are summarized in Fig. 4. The time zero in Fig. 4 represents the time when the specimens were demolded 6 hours after casting. The data show the shrinkage strain of each material at the ages of 1, 3, 7, 28, and 60 days. It should be noted that the HES-ECC mixture had the highest shrinkage value because of higher cement content and the absence of large coarse aggregates; the HES-SFRC mixture

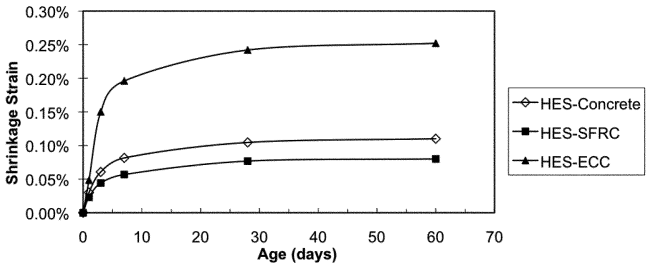

Fig. 4—Free shrinkage strain of repair materials at different ages.

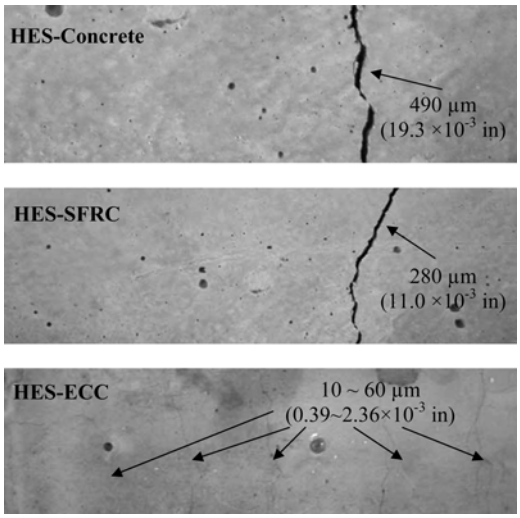

Fig. 5—Repair surface cracking at age of 60 days.

had the lowest shrinkage strain value because of the constraint effect of steel fibers.[29]

The cracking potential p (Eq. (1) and (5)) for HES-concrete, HES-SFRC, and HES-ECC at the age of 28 days can be estimated based on measured values of ε_{sh} and ε_i shown in Table 5. The other parametric values (ε_e and ε_{cp}) were not measured in this study, but were adopted for estimation as the ε_e and ε_{cp} of normal concrete and SFRC from Li.[24] Although HES-ECC had the highest shrinkage, its negative p-value verifies that HES-ECC remains in the strain-hardening stage under restrained drying shrinkage, and will experience microcracking damage without fracture localization. In contrast, HES-concrete and HES-SFRC are subjected to tensile fracturing due to their positive p-values.

Surface cracking and interface delamination of repaired systems

Table 6 summarizes the surface crack pattern—crack number and crack width of the three repaired systems, respectively, at the age of 60 days. Three specimens were tested for each repair material. When the HES-concrete was used as the repair material, three to four surface cracks localized at the age of 60 days. The maximum crack width of the three specimens was 490 μm (19.3×10^{-3} in). When the HES-SFRC was used as the repair material, one to four localized surface cracks formed, and the maximum crack width of the three specimens was 280 μm (11.0×10^{-3} in.). The smaller crack width of the HES-SFRC can be attributed to the steel fibers' bridging effect. The crack widths for the HES-concrete or HES-SFRC repair layers is a structural property, which is dependent on structural dimensions.

Table 5—HES-concrete, HES-SFRC, and HES-ECC cracking potential estimation (properties were measured at specimen age of 28 days)

Properties	ε_{sh}, %	ε_e, %*	ε_i, %	ε_{cp}, %*	$p = [\varepsilon_{sh} - (\varepsilon_e + \varepsilon_i + \varepsilon_{cp})]$, %
HES-concrete	0.105	0.01	0	0.02 to 0.06	0.035 to 0.075
HES-SFRC	0.077	0.01	0	0.02 to 0.06	0.007 to 0.047
HES-ECC	0.242	0.015	3 to 5	0.07	–4.843 to –2.843

*ε_e and ε_{cp} were adopted for estimation as ε_e and ε_{cp} of normal concrete and SFRC from Billington and Rouse[18] and Li.[24]

Table 6—Interface delamination and surface cracking of different layered repair systems at age of 60 days

Repair material	Specimen number	Delamination		Surface cracking	
		Height, μm (in. × 10^{-3})	Length, mm (in.)	Number	Width, μm (in. × 10^{-3})
HES-concrete	(1)	90 (3.54)	170 (6.69)	3	160 (6.30), 520 (20.5), 370 (14.6)
	(2)	30 (1.18)	27 (1.06)	4	190 (7.48), 340 (13.4), 360 (14.2), 490 (19.3)
	(3)	65 (2.56)	73 (2.87)	4	700 (2.76), 380 (15.0), 420 (16.5), 450 (17.7)
HES-SFRC	(1)	310 (12.2)	323 (12.72)	2	110 (4.33), 120 (4.72)
	(2)	260 (10.2)	301 (11.85)	4	50 (1.97), 90 (3.54), 120 (4.72), 130 (5.12)
	(3)	300 (11.8)	342 (13.46)	1	280 (11.0)
HES-ECC	(1)	80 (3.15)	82 (3.23)	83	10 to 50 (0.39 to 1.97)
	(2)	50 (1.97)	47 (1.85)	109	10 to 60 (0.39 to 2.36)
	(3)	75 (2.95)	79 (3.11)	113	10 to 50 (0.39 to 1.97)

For the HES-ECC repair material, 83 to 113 microcracks were found on the surface of the repair layer, with the maximum crack width of 60 μm (2.36×10^{-3} in.), much tighter than that of the HES-concrete or HES-SFRC repair layers. The average crack width of the HES-ECC repair was around 30 μm (1.18×10^{-3} in.). No localized fracture was observed. Because the shrinkage strain of the HES-ECC was less than 0.3% (Fig. 4), substantially below its tensile strain capacity of 2.5 to 5%, the restrained shrinkage cracking of the HES-ECC occurred in its strain-hardening stage, during which the material formed multiple microcracks with steady-state crack width. Thus the restrained shrinkage crack width in the HES-ECC repair layer is a material property independent of structural dimensions.[24] Even for larger scale or field repair applications with different types of restrained conditions, the HES-ECC repair is still expected to exhibit a tight crack width below 60 μm (2.36×10^{-3} in.) as long as the imposed total strain level does not exceed the strain capacity of the HES-ECC material. This tight crack width can greatly reduce transport by permeation[30] and chloride penetration.[31] The tight crack width performance has been observed in an ECC bridge deck patch repair.[25]

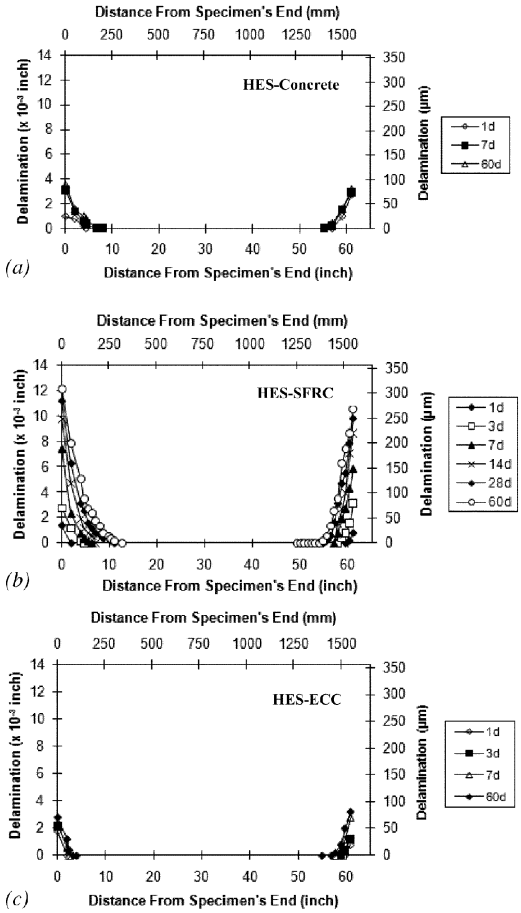

Fig. 6—Interface delamination profile of: (a) HES-concrete; (b) HES-SFRC; and (c) HES-ECC repaired systems.

Figure 5 shows the surface cracking pattern of each type of repair layers. The HES-concrete and HES-SFRC repairs exhibited localized fractures, in contrast to the multiple microcracks of HES-ECC repair with significantly smaller crack widths.

The measured interface delamination height and length of the nine layered repair specimens are summarized in Table 6. As illustrated in Fig. 1, the delamination height is the distance between the crack faces of the crack running along the repair-substrate boundary, at the two ends of the repaired system; the delamination length is the length of the delaminated section along the long axis of the specimen. At the age of 60 days, both the HES-ECC and the HES-concrete repaired systems exhibited relatively low delamination heights at the specimen ends, which were 80 μm (3.15×10^{-3} in.) for the former and 90 μm (3.54×10^{-3} in.) for the latter at the maximum. The maximum delamination length was 82 mm (3.23 in.) for the HES-ECC repair and 170 mm (6.69 in.) for the HES-concrete repair at the maximum. The HES-SFRC repaired system had much larger delamination height than the HES-ECC or HES-concrete repaired system at the age of 60 days, which was 310 μm (12.2×10^{-3} in.). Its delamination length was also larger, around 340 mm (13.46 in.). Figure 6 shows the interface delamination profiles (delamination height as a function of position along the repair/substrate interface) of the three layer repair systems at different ages. As expected, these profiles are approximately symmetric about the midpoint of the specimen.

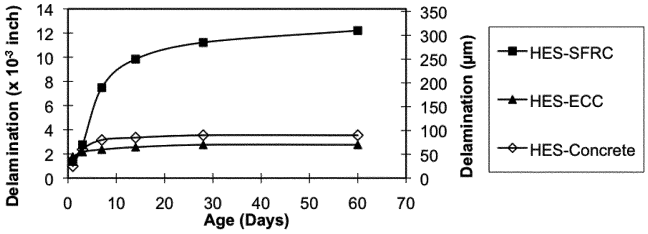

Fig. 7—Specimen end delamination height at different ages.

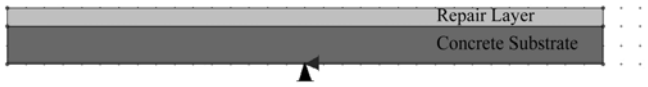

Fig. 8—FEM model of layered repair system.

For each of the three repaired systems, the averaged values of interfacial delamination height at both ends as a function of time are shown in Fig. 7. It can be seen that the HES-ECC and HES-concrete repaired systems completed most of their interface delamination at early ages—within 7 days, when surface cracking has already been completed and helped to release tensile and shear stresses at the specimen interface. For the SFRC repaired system, however, delamination continued to evolve up to 60 days, at which time the SFRC repair material had undergone most of its shrinkage (Fig. 4). This further confirms that the fiber-bridged cracks of the HES-SFRC repair could only release part of the stresses at the interface, so that delamination continued as shrinkage went on. As can be seen, the HES-SFRC repair exhibited interface delamination height three to four times higher than the other two repair materials.

It should be noted that the contrasting behavior between the three repair materials studied herein depends on the degree of restraint. The degree of restraint in the studied system is relatively low as the concrete substrate cross section is not significantly larger than that of the repair layer. In situations such as surface repair of a large girder, the degree of restraint would be higher; the contrast of the repair layer response between the three repair materials is expected to be even higher.

ANALYTICAL INVESTIGATION

Problem formulation and FEM model

A numerical study was carried out to simulate the layered repair specimen by using a finite element multi-layer systems (MLS) computer software program[32] that calculates drying shrinkage and/or temperature-induced stresses in multilayer systems. The module MLS can compute physical and structural behavior of composite structure, taking into account varying environmental conditions.

In this numerical study, a concrete substrate is considered that has been repaired by a freshly cast layer of material. The dimensions of the concrete substrate and the repair layer adopted are the same as those of the experimental specimen. The geometry and mechanical boundary conditions of this model are shown in Fig. 8.

Three material models were applied respectively to simulate the three types of repair material: brittle material model—HES-Concrete; tension softening model—HES-SFRC; and strain hardening model—HES-ECC (Fig. 9). In these models, a bilinear stress-strain relation was used to describe the elastic straining and strain-hardening response, while a

Table 7—Interface property* values assumed in FEM model

f_t	4.0 MPa (580 psi)
Factor for S_1	0.25
w_1	0.05 mm (2.0×10^{-3} in.)
w_2	0.2 mm (7.9×10^{-3} in.)
Friction angle	35.0 degrees
Maximum slip	3.0 mm (0.12 in.)
Normal stiffness	100 N/mm^3 (3.7×10^5 lb-f/in.^{3})
Shear stiffness	10 N/mm^3 (3.7×10^4 lb-f/in.^{3})

*Interface parameters f_t, S_1, w_1, and w_2 are denoted in Fig. 10.

stress-crack opening relation was used to describe the tension-softening response. Note that the parameters of the material models were age-dependent and were fitted as curves according to experimentally measured results from material age of 4 hours to 28 days obtained in the present study. For example, the initial slope of the three curves—the material Young's modulus E changed with material ages according to experimental results as shown in Tables 3 and 4. The age-dependent tensile strength of the HES-ECC was adopted from the testing results in Table 4. The first cracking strength of the HES-ECC was assumed to be 80% of the ultimate tensile strength, determined based on the uniaxial tensile stress-strain curves of the HES-ECC measured at different ages. Because the purpose of this numerical study was to evaluate the effect of material ductility on repair performance, the tensile strength of all three materials was assumed the same at all ages. Statistical standard deviation of material tensile strength of the three materials was assumed to be 10% of the average tensile strength in the finite-element-method (FEM) model for the repair layers. The tensile strain capacity of the HES-ECC was conservatively assumed to be 3% at all ages. Compressive strength of the three materials adopted the experimental data in Table 3. The Poisson's ratio was assumed the same (0.2) for all materials.

The concrete substrate was assumed to have the same mechanical and fracture properties as the HES-concrete repair layer. No cracking and shrinkage was considered in the old concrete substrate.

The repair/old concrete interface used the interface Type A model defined in the computer software,[32] with properties listed in Table 7 and illustrated in Fig. 10. No direct measurements were made of the interface properties, but were assumed to be the same in all three repair material cases. The interface tensile strength f_t was assumed to be 4 MPa (580 psi)[23] but the residual tensile capacity across the interface varies with tensile opening and shear slip, as illustrated in Fig. 10. Note that the interface model parameters as recommended by the computer software program [32] are assumed constant in time, but is not expected to be the case in reality. Hence, the prediction of interface delamination is only an approximation. Further research is needed to quantify the time-dependent interfacial properties for the three cases.

In this numerical model, the loading on the system was derived from the repair material drying shrinkage that changed with age. The measured shrinkage strain of the HES-concrete, HES-SFRC, and HES-ECC shown in Fig. 4 were used as the input loading for this FEM model. As

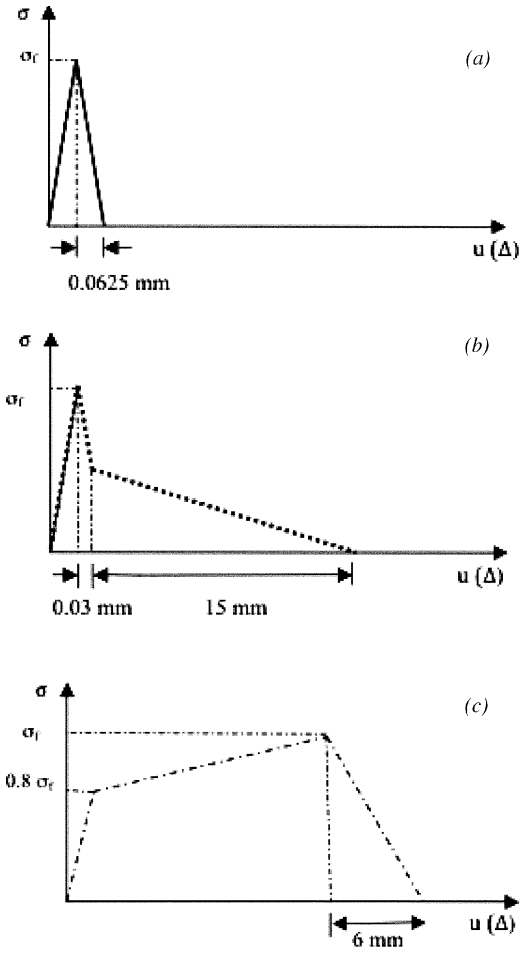

Fig. 9—Assumed tensile behavior of: (a) HES-concrete; (b) HES-SFRC; and (c) HES-ECC materials.

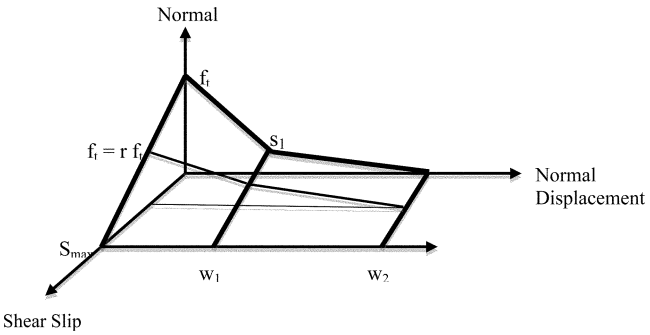

Fig. 10—Interface model: combined uniaxial stress-strain relation in the normal direction with influence of shear slip.

expected, the top surface of the repair layer experienced free shrinkage, but the material built up stress as it approached the interface with the restraining substrate. The computer software program[32] accounts for this by the prescribed geometry of the layer and the substrate, and the assumption that the substrate remains elastic with no change in property with time.

Numerical simulation results

The FEM model predicted cracking behavior of the HES-concrete, HES-SFRC, and HES-ECC repairs at 60 days is shown in Fig. 11. The HES-concrete repair developed several localized

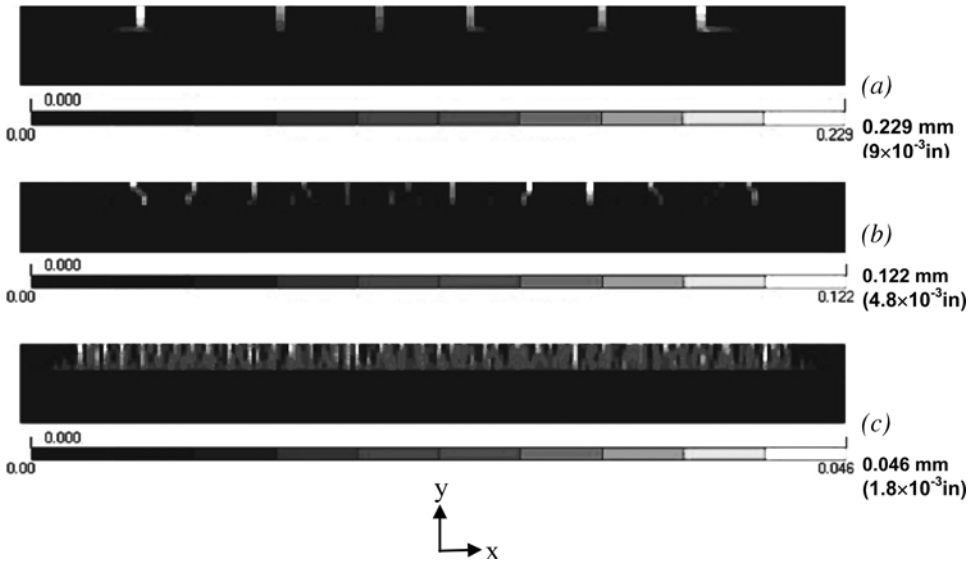

Fig. 11—Predicted crack width of: (a) HES-concrete, (b) HES-SFRC and (c) HES-ECC repair layer at the age of 60 days.

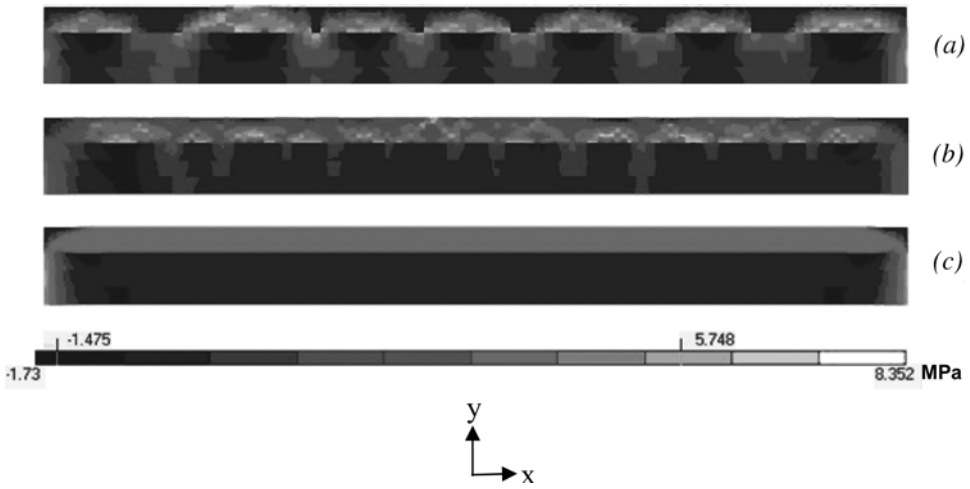

Fig. 12—Predicted stress (σ_{xx}) distribution in: (a) HES-concrete; (b) HES-SFRC; and (c) HES-ECC repaired system at age of 60 days.

cracks with a maximum crack width of 229 μm (9×10^{-3} in.). The HES-SFRC repair layer developed more localized cracks, but smaller maximum crack width of 122 μm (4.8×10^{-3} in.). Despite the nearly three times higher shrinkage strain of the HES-ECC compared with the HES-concrete and the HES-SFRC, the HES-ECC exhibited "saturated" cracking behavior with crack width under 46 μm (1.8×10^{-3} in.). These results from FEM model simulation are consistent with the experimental results (Table 6 and Fig. 5). Although the cracking numbers predicted by the FEM models are not exactly the same as the experimental results due to the unavoidable material variability (for example, initial flaw sizes), simplified model, and uncertain assumptions, the cracking trends (localized fractures with larger crack width in the HES-concrete and the HES-SFRC repairs and microcracks in the HES-ECC repair) are accurately predicted by the FEM model.

Figure 12 shows the tensile stress σ_{xx} distribution in the HES-concrete, HES-SFRC, and HES-ECC repair layers at the age of 60 days. Figure 13 shows the repair/old interface shear stress (σ_{xy}) distribution of the three repaired systems at the age of 60 days. In the HES-concrete repair, σ_{xx} is zero at the cracking locations because the cracks are traction-free. Opening these cracks relieves part of interface normal and shear stresses, and reduces interface delamination at the ends of repair. It can be seen from Fig. 13, however, that σ_{xy} remains at a significant level. The tensile component σ_{yy} (not shown) shows a similar trend. This high stress is due to the tendency of shrinking for the repair elements between the widely separated cracks, but is restrained by the underlying substrate. Therefore, although the HES-concrete repair exhibited a similar amount of interface delamination as the HES-ECC repair in the experiments, the FEM model simulation indicates that the tendency of interface delamination of the HES-concrete repair is much higher than the HES-ECC repair due to the higher level of interface stresses, which is induced by the continued shrinkage of HES-concrete repair segments between localized cracks. In the HES-SFRC repair, σ_{xx} is non-zero at the cracking locations due to steel fiber bridging. The resulting high interface stresses (Fig. 13) induce high interface delamination in the HES-SFRC repair.

A significantly different behavior can be observed in the HES-ECC repair. The "saturated" microcracks of the HES-ECC

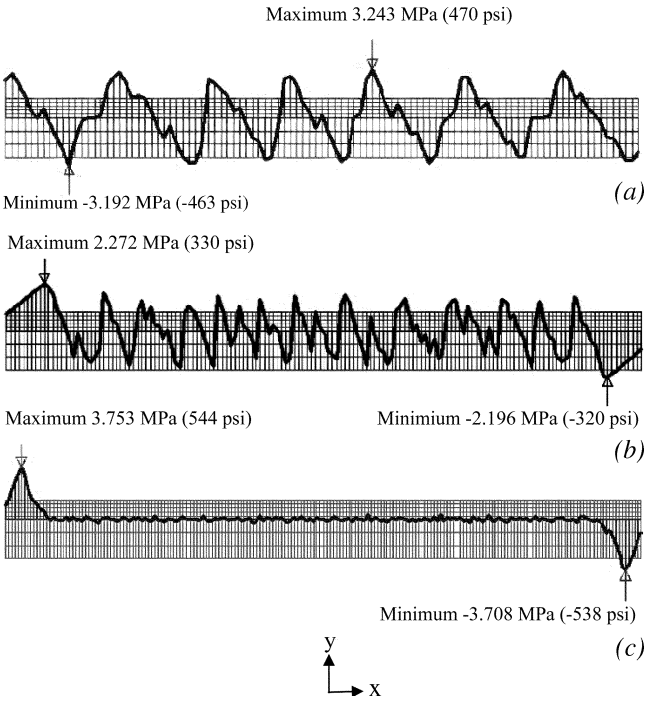

Fig. 13—Predicted interface shear stress (σ_{xy}) of: (a) HES-concrete; (b) HES-SFRC; and (c) HES-ECC repaired system at age of 60 days.

are tight (below 46 μm [1.8×10^{-3} in.]) and uniformly distributed through the repair layer. After cracking, these microcracks can still carry a significant amount of stress, as seen in Fig. 12. By developing a large number of microcracks, the HES-ECC repair deforms uniformly in a ductile manner, and relieved the stresses everywhere along the interface. Thus, the "plastic" straining of the ECC repair layer accommodated the shrinkage deformation. Figure 13 shows that the shear stress σ_{xy} (and similarly the tensile stress σ_{yy}, not shown) distribution is, more or less, uniform along the interface. A small amount of interface delamination exists only at the repair ends. The HES-ECC repair layer surface cracking and interface delamination behavior experimentally measured and numerically computed in this study are consistent with those numerically modeled by Kabele.[23]

CONCLUSIONS

Based on the results of this experimental and numerical investigation of a layered repair system with three types of repair materials, the following conclusions can be drawn:

1. When subject to restrained drying shrinkage, many fine microcracks (over 100) with tight crack width form in the HES-ECC repair layer, with a small amount of interface delamination. In contrast, a few large surface cracks form in the HES-concrete repair layer while large interface delamination forms in the HES-SFRC repaired system. Corroborated by numerical analyses, this finding supports the contention that HES-ECC with high tensile ductility offers the strongest likelihood for attaining durable concrete structure repairs with relatively small delamination length and tight surface crack width. The underlying reason for the advantageous performance of HES-ECC is the presence of a unique large inelastic strain capacity to offset shrinkage demand.

2. The FEM model study confirms the contrasting response of the three different repair materials and the advantage of having a large inelastic strain capacity in HES-ECC to minimize both surface crack width and delamination length and height. The analyses provide additional insights on the internal stress distribution (not available experimentally) in the repair layer induced by restrained shrinkage and surface cracking and interface delamination.

3. Repair material ductility is closely related to cracking potential p under restrained volume change such as shrinkage or thermal effect. In this sense, in repair materials engineering and in concrete repair design guides, repair material ductility, not compressive strength, should be given the most significance. When the repair material ductility requirement is satisfied, material free shrinkage limit becomes less important, while surface preparation methods to enhance interfacial bond to further reduce interfacial delamination of the HES-ECC repair will be more meaningful on achieving durability of repaired concrete structures.

It should be pointed out that repair failures result from various causes, including thermal and steel corrosion effects. The study of these effects is outside the scope of this paper as it focuses only on the major cause associated with restrained drying shrinkage of the repair layer.

ACKNOWLEDGMENTS

This work is partially supported by a grant from the Michigan Department of Transportation and by a fellowship to M. Li from the University of Michigan. The authors would like to thank E. Schlangen at Delft University of Technology for sharing with us his knowledge in FEMMASSE and its applications.

REFERENCES

1. Vaysburd, A. M.; Brown, C. D.; Bissonnette, B.; and Emmons, P. H., "'Realcrete' versus 'Labcrete,'" *Concrete International*, V. 26, No. 2, Feb. 2004, pp. 90-94.

2. Mather, B., and Warner, J., "Why Do Concrete Repairs Fail," Interview held at University of Wisconsin Department of Engineering, Professional Development (http://aec.engr.wisc.edu/resources/rsrc07.html), accessed Nov. 2003.

3. Emmons, P. H.; Vaysburd, A. M.; and McDonald, J. E., "A Rational Approach to Durable Concrete Repairs," *Concrete International*, V. 15, No. 9, Sept. 1993, pp. 40-45.

4. Emberson, N. K., and Mays, G. C., "Significance of Property Mismatch in the Patch Repair of Structural Concrete, Part 1: Properties of Repair Systems," *Magazine of Concrete Research*, V. 42, No. 152, 1990, pp. 147-160.

5. Emmons, P. H., "Concrete Repair and Maintenance Illustrated," ASTM International, West Conshohocken, PA, 1994, pp. 155-164.

6. Emmons, P. H., "System Concept in Design and Construction of Durable Concrete Repairs," *Construction and Building Materials*, V. 10, No. 1, 1996, pp. 69-75.

7. ACI Committee 224, "Control of Cracking in Concrete Structures (ACI 224R-01)," American Concrete Institute, Farmington Hills, MI, 2001, 45 pp.

8. Gowripalan, N.; Sirivivatnanon, V.; and Lim, C. C., "Chloride Diffusivity of Concrete Cracked in Flexure," *Journal of Cement and Concrete Research*, V. 30, No. 5, May 2000, pp. 725-730.

9. Kriviak, G. W.; Skeet, J. A.; and Carter, P. D., "Service Life Prediction of Protective Systems for Concrete Bridge Decks in Alberta," International Association of Bridges and Structural Engineers Symposium, San Francisco, CA, 1995, pp. 469-474.

10. Tanaka, Y.; Kawano, H.; Watanabe, H.; and Nakajo, T., "Study on Required Cover Depth of Concrete Highway Bridges in Coastal Environment," 17th U.S.-Japan Bridge Engineering Workshop, Tsukuba, 2001.

11. Li, V. C., "From Micromechanics to Structural Engineering—the Design of Cementitious Composites for Civil Engineering Applications," *JSCE Journal of Structural Mechanics and Earthquake Engineering*, V. 10, No. 2, 1993, pp. 37-48.

12. Li, V. C., "Advances in ECC Research," *Concrete: Materials Science to Application, A Tribute to Surendra P. Shah*, SP-206, P. Palaguru, A. Naaman, and W. Weiss, eds., American Concrete Institute, Farmington Hills, MI, 2002, pp. 373-400.

13. Li, V. C.; Wu, C.; Wang, S.; Ogawa, A.; and Saito, T., "Interface Tailoring for Strain-Hardening PVA-ECC," *ACI Materials Journal*, V. 99, No. 5, Sept.-Oct. 2002, pp. 463-472.

14. Li, V. C., and Hashida, T., "Engineering Ductile Fracture in Brittle Matrix Composites," *Journal of Materials Science Letters*, V. 12, 1993, pp. 898-901.

15. Li, V. C.; Mishra, D. K.; and Wu, H. C., "Matrix Design for Pseudo Strain-Hardening Fiber Reinforced Cementitious Composites," *RILEM Materials and Structures Journal*, V. 28, No. 183, 1995, pp. 586-595.

16. Kim, Y. Y.; Fischer, G.; Lim, Y. M.; and Li, V. C., "Mechanical Performance of Sprayed Engineered Cementitious Composite (ECC) Using Wet-Mix Shotcreting Process for Repair," *ACI Materials Journal*, V. 101, No. 1, Jan.-Feb. 2004, pp. 42-49.

17. Kamada, T., and Li, V. C., "The Effects of Surface Preparation on the Fracture Behavior of ECC/Concrete Repair System," *Journal of Cement and Concrete Composites*, V. 22, No. 6, 2000, pp. 423-431.

18. Billington, S., and Rouse, J. M., "Time-Dependent Response of Highly Ductile Fiber-Reinforced Cement Based Composites," in *Proceedings*, BMC-7, Warsaw, Poland, A. M. Brandt, V. C. Li, and I. H. Marshall, 2003, pp. 47-56.

19. Wang, S., and Li, V. C., "High-Early-Strength Engineered Cementitious Composites," *ACI Materials Journal*, V. 103, No. 2, Mar.-Apr. 2006, pp. 97-105.

20. Li, M., and Li, V. C., "Durability of HES-ECC Repair Under Mechanical and Environmental Loading Conditions," *Proceedings, High Performance Fiber Reinforced Cement Composites*, H. W. Reinhardt and A. E. Naaman, eds., Mainz, Germany, 2007, pp. 399-408.

21. Wittmann, F. H., and Martinola, G., "Decisive Properties of Durable Cement-Based Coatings for Reinforced Concrete Structures," *International Journal for Restoration of Buildings and Monuments*, V. 9, No. 3, 2003, pp. 235-264.

22. Li, V. C., and Stang, H., "Elevating FRC Material Ductility to Infrastructure Durability," *Proceedings of BEFIB*, Varenna, Lake Como, Italy, Sept. 2004, pp. 171-186.

23. Kabele, P., "Assessment of Structural Performance of Engineered Cementitious Composites by Computer Simulation," *CTU Report 4*, Czech Technical University, Prague, 2001.

24. Li, V. C., "High Performance Fiber Reinforced Cementitious Composites as Durable Material for Concrete Structure Repair," *International Journal for Restoration of Buildings and Monuments*, V. 10, No. 2, 2004, pp. 163-180.

25. Lepech, M. D., and Li, V. C., "Long Term Durability Performance of Engineered Cementitious Composites," *Journal of Restoration of Buildings and Monuments*, V. 12, No. 2, 2006, pp. 119-132.

26. Stang, H., "Scale Effects in FRC and HPRFCC Structural Elements," *High Performance Fiber Reinforced Cementitious Composites*, RILEM Proceedings Pro 30, A. E. Naaman and H. W. Reinhardt, eds., 2003, pp. 245-258.

27. ASTM C157/C157M, "Standard Test Methods for Length Change of Hardened Hydraulic-Cement Mortar and Concrete," ASTM International, West Conshohocken, PA, 1999, 7 pp.

28. ASTM C596, "Standard Test Method for Drying Shrinkage of Mortar Containing Hydraulic Cement," ASTM International, West Conshohocken, PA, 2001, 3 pp.

29. Grzybowsk, M., and Shah, S., "Shrinkage Cracking of Fiber Reinforced Concrete," *ACI Materials Journal*, V. 87, No. 2, Mar.-Apr. 1990, pp. 138-148.

30. Lepech, M., and Li, V. C., "Water Permeability of Cracked Cementitious Composites," *Paper* 4539 of Compendium of Papers, ICF 11, Turin, Italy, Mar. 2005. (CD-ROM)

31. Sahmaran, M.; Li, M.; and Li, V. C., "Transport Properties of Engineered Cementitious Composites Under Chloride Exposure," *ACI Materials Journal*, V. 104, No. 6, Nov.-Dec. 2007, pp. 604-611.

32. "FEMMASSE MLS: Computer Program for the Analysis of the Thermal and Mechanical Behavior of Hardening Concrete," User Manual, 2006.